# Supporting Information

## All-solid-state disordered $LiTiS_2$ pseudocapacitor

*Justin M. Whiteley, Simon Hafner, San Sub Han, Seul Cham Kim, Viet-Duc Le, Chunmei Ban, Yong Hyun Kim, Kyu Hwan Oh, Se-Hee Lee**

To probe the diffusivity of the prepared $TiS_2$ variants, the galvanostatic intermittent titration technique (GITT) is used. The GITT technique was developed by Weppner and Huggins[1] and furthered by Wen et al.[2] This technique applies a current pulse to the system and measures the relaxation voltage. The calculation is given by **Equation S1**:

$$D_{Li} = \frac{4}{\pi\tau} L^2 \left( \frac{\Delta E_s}{\Delta E_t} \right)^2 \qquad t << \frac{L^2}{D} \tag{S1}$$

Where $\tau$ is the time of the current pulse, $L$ is the length of the electrode, $\Delta E_s$ is the change in steady-state voltage as a result of the current pulse, and $\Delta E_t$ is the total change in voltage during the application of constant current (subtracting out uncompensated ohmic effects).[2] GITT is performed by using a rate of C/20 for 1 hour followed by a 6 hour relaxation over the voltage range of 3 to 1 V on the third cycle. **Figure S1** displays the result of GITT experiment. Both *b*TS and *n*LTS display the familiar characteristics of the *1T* variant. This includes a low initial coefficient responding to initial separation of S-Ti-S slabs with increasing lithium. Once sufficient space is developed in the van der Waals gap, $D_{Li}$ is increased to a maximum at approximately 0.6 moles of Li in $Li_xTiS_2$. A decline is $D_{Li}$ is then observed as the octahedral sites in the van der Waals gap is completely saturated with Li.[3] *d*LTS has very different characteristics. An extremely high $D_{Li}$ is observed at initial stages of lithiation followed by a decrease. This could indicate that due to the disordered nature of *d*LTS, Li does not act to expand the van der Waals gap. Thus the decrease in $D_{Li}$ would respond to higher levels of Li saturation.

A maximum in $D_{Li}$ is again observed at the same level as *n*LTS. Differing from the other samples, instead of a sharp dropoff in $D_{Li}$, a constant is achieved. The constant could be related to diffusion along the surface of the S-Ti-S slabs. Once the surface of these slabs begin to saturate, a dropoff is again seen in $D_{Li}$.

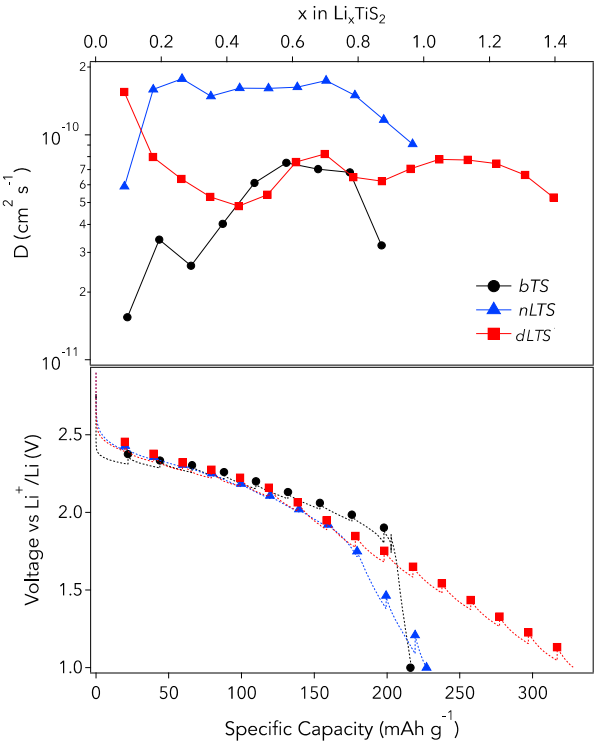


**Figure S1.** GITT for the three samples. (Upper) Computed diffusion coefficents. (Lower) Voltage profile with relaxed voltages in the solid markers. Both *b*TS and *n*LTS display well known trends in diffusion coefficient where a maximum is achieved around 0.6 moles of Li, while simultaneously achieving theoretical capacity. *d*LTS has an undocumented trend with a stable, high diffusion coefficient far past the thermodynamic limit for the material.

**Figure S2** displays electron energy loss spectroscopy (EELS) of the cross-section developed in Figure 1 of *d*LTS. The particles, having been detailed to be in the 50-300 nm range in Figure 1d, are visible as the dark domains in Figure 2a. The S-K and Ti-K signals (Figure S2b and S2c, respectively) are present in the dark domains; however, the Li-K signal (Figure S2d) is confined to the what appears the particle boundaries and what appears the much lighter domains in Figure S2a. Therefore, it is concluded that the lithium reacts with the Ga ion milling to form

on the surface of the particles, which is consistent with literature.[4] Due to high mobility of Li in *d*LTS, we do not expect this phenomenon to significantly alter the structure detected by HR-TEM in Figure 1.

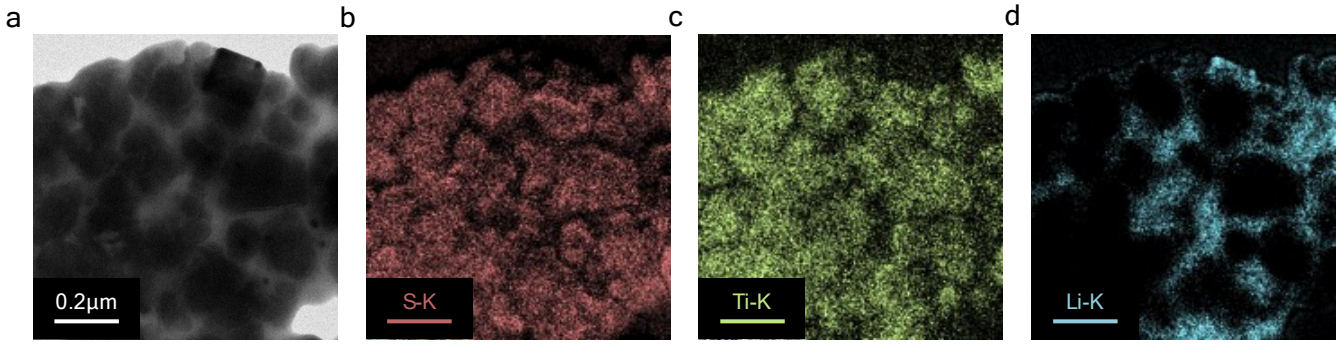


**Figure S2.** a) SEM of *d*LTS cross-section prepared by Ga ion FIB mill. b) S-K EELS signal. c) Ti-K EELS signal. d) Li-K EELS signal. It appears that Li reacts with the milling process acting to deintercalate the material, forming a lithium matrix around the $TiS_2$ material.

CVs in the voltage range of 3 to 1 V for *b*TS, *n*LTS and *d*LTS at 60°C are displayed in **Figure S3a** to S3c and at 120°C in S3d to S3f, respectively. The large shifts in redox peaks in *b*TS at 60°C in Figure S3a are much larger than those reported in liquid cells. These shifts in both cathodic and anodic peaks are a result of large uncompensated resistance of the solid electrolyte layer.[5] Typically, liquid electrolyte resistance are almost 10 times less resistive than a solid electrolyte layer, therefore, the temperature is raised to 120°C for proper response. It is clear that once the CV is performed at 120°C for *b*TS in Figure S3d, no large increase in capacitance is observed in the 1 to 2 V region. This could indicate the capacitive response is not a result of the elevated temperature but a material response. *n*LTS in Figure S3b and S3e has a similar behavior to *b*TS but with a larger peak shift. This could be the result of access to more material at the higher rates as both samples contain the same amount of material. A small rectangular portion is exhibited near 1 V during sweep rate reversal. This small pseudo-capacitive effect has been documented in nano $LiTiS_2$ previously.[6] *d*LTS exhibits the largest

shift in cathodic voltage with scan rate in Figure S3f. This is typical for a large activation energy as the anodic peak does not undergo the same shift[5] This same shift is present at elevated temperatures (Figure S3f) with a smaller degree. During sweep rate reversal, a sharp increase in current response occurs followed by a reversible peak at the same voltage for all rates. This has been a well documented pseudo-capacitive effect.[7]

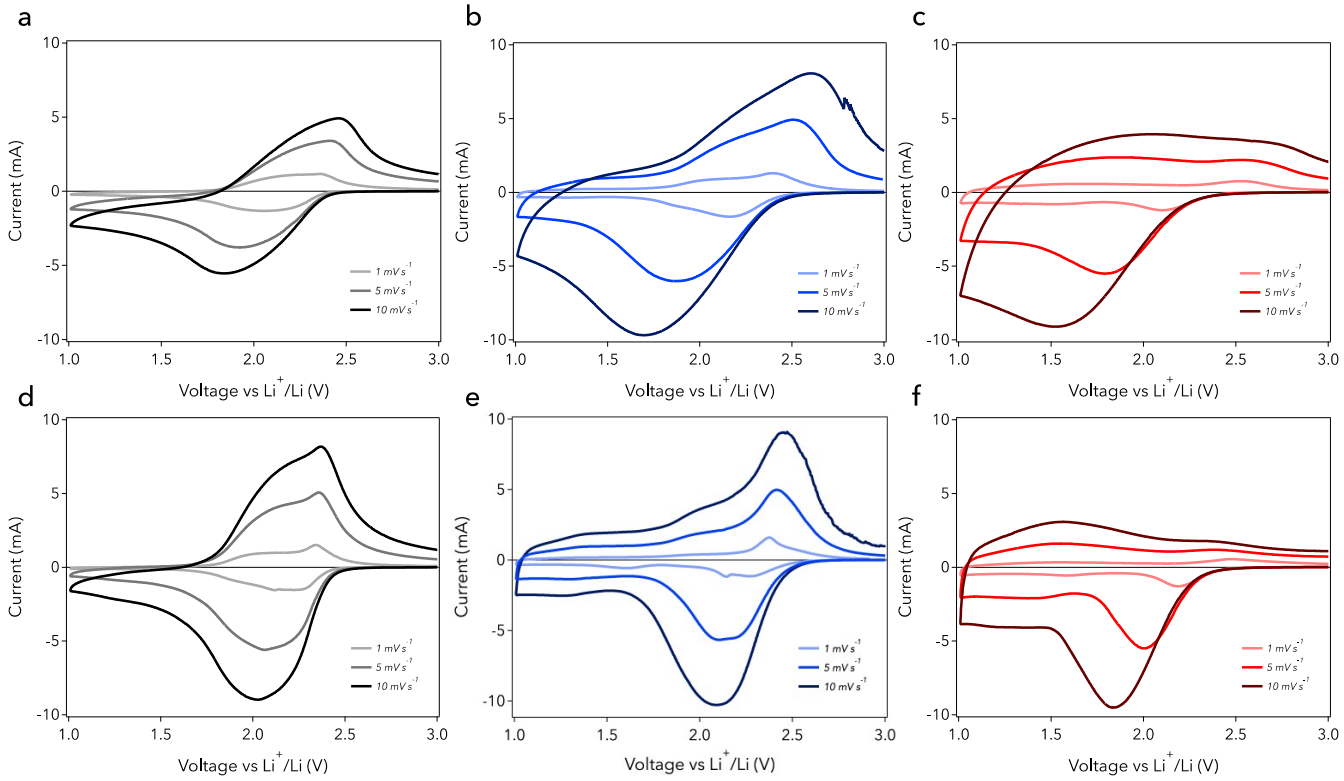


**Figure S3.** CVs over a 3 to 1 V range at 60°C for a) *b*TS, b) *n*LTS, c) *d*LTS. The same tests performed at 120°C for a) *b*TS, b) *n*LTS, c*) d*LTS. While *b*TS and *n*LTS have similar shapes, the more nano *n*LTS is able to achieve greater delivered current in the solid-state. At the same time, larger peak shifts are identified in *n*LTS. *d*LTS has a completely different form at both temperatures.

**Figure S4a** and S4b are CVs in the range of 1 to 2 V at 120°C for *b*TS and *n*LTS, respectively, the same test as performed in Figure 1c displaying a sharp contrast. *b*TS does not display any pseudocapacitance in this range. The cathodic and anodic response appears to be a result of delithiation and lithiation of the diffusive type indicated by a cathodic peak following the anodic response that displays a voltage shift.[5] *n*LTS displays more pseudocapacitance with

the longer plateau of current developing into two stages essentially. There still appears to to be some diffusive response near 2 V which is adding to the overall calculated capacitance value in Figure 2d. It is unclear if this pseudocapacitance is surface redox as demonstrated by *d*LTS or intercalation pseudocapacitance as previously reported.[6]

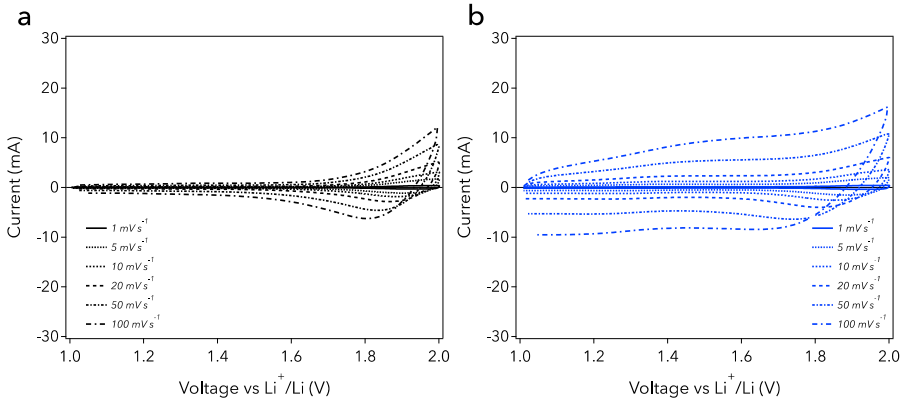


**Figure S4.** CVs over a 1 to 2 V range at 120°C for a) *b*TS, b) *n*LTS. The behavior developed near 2 V are clearly diffusive in nature due to peaks present on the the cathodic sweep following anodic sweep. This diffusive region adds to the specific capacitance values calculated in Figure 1 and are incorrect in referring to a capacitance value.

**Figure S5a** are CVs for *d*LTS in the 1 to 2 V range at a variety of temperatures. This is to determine if by raising the temperature to 120°C for testing has any significant effect on *d*LTS characteristics. For all temperatures, specific capacitance is not significantly affected by temperature and *d*LTS still exhibits strong pseudocapacitance (over 300 F $g^{-1}$ in Figure S5b) at 60°C. While the current derived increases slightly with temperature, there is also a change in the steepness of current reversal during sweep rate reversal at 2 V. This has been reportedly due to uncompensated resistances in the design cell which demonstrates that raising conductivity in the solid electrolyte, provides a better response for determining pseudocapacitance in the solid-state.

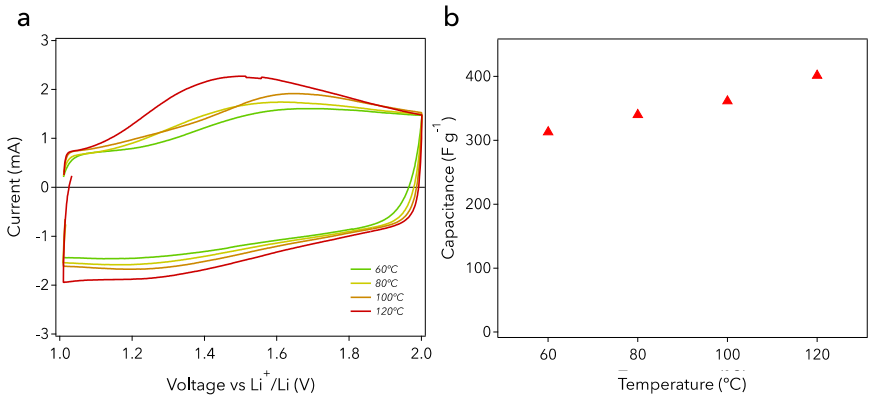


**Figure S5.** a) CV of *d*LTS over a 1 V range at various temperatures, b) Computed capacitance values for increasing temperatures. While slight amounts of capacitance are added with increasing temperature, the relative shape of the CV is almost unchanged. A large effect is seen during the switch from anodic to cathodic current. Increasing temperature reduces the uncompensated resistance and increases the vertical nature of this switch.

**Figure S6** pertains to additional information for cycling in Figure 2. The coulombic efficiency for *d*LTS over the course of cycling at C/2 is displayed in Figure S6a. Taking a fit, the average CE is 99.7%. Some variation can be due to small temperature fluxations in the oven used to operate the cells at 60°C. Figure S6b, S6c, and S6d are voltage profile evolutions for *d*LTS, *n*LTS, and *b*TS, respectively, in Figure 2a. *d*LTS keeps its distinct shape over the course of the 1000 cycles including the pseudocapacitive range. Both *n*LTS and *b*TS exhibit a plateau shortening and rising ohmic overpotential. Possible explanations for the better cycling stability include lower volumetric changes in *d*LTS due to disordering and smaller domain sizes, and lower active material isolation in *d*LTS due to more isotropic diffusion of lithium.

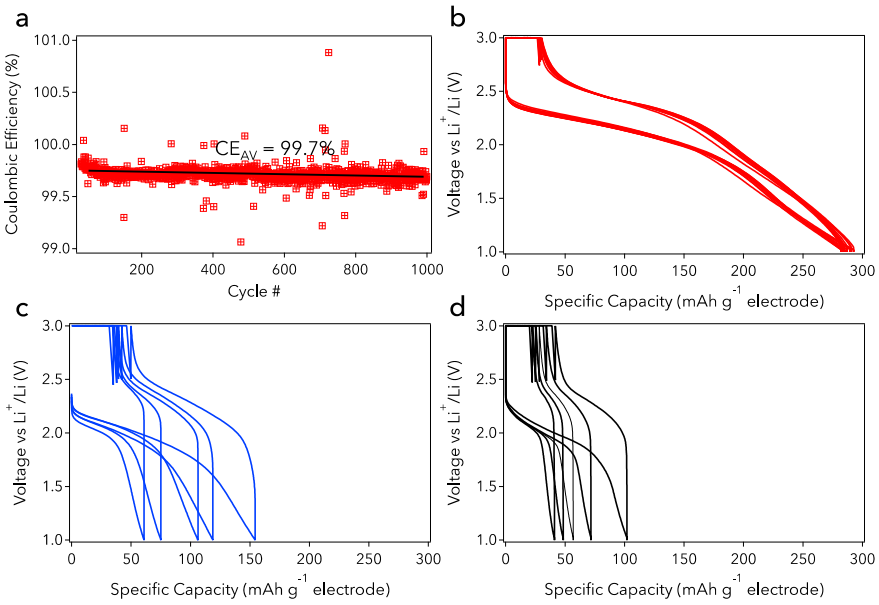


**Figure S6**. a) CE over the course of cycling at C/2 for *d*LTS. b) Voltage profile evolution (every 100 cycles) for at C/2 for b) *d*LTS, c) *n*LTS, d) *b*TS. The pseudocapacitive region for *d*LTS is present throughout the 1000 cycles.

The effects of cycling purely in the pseudocapacitve range for *d*LTS is investigated (**Figure S7**). A rate study is performed up to 20C (1.44 A $g^{-1}$), the highest ever reported for a solid-state cell. The voltage sweeps in the 2 to 1 V range are displayed in Figure S7a. Extended cycling is then carried out at 2C (0.28 A $g^{-1}$) for 750 cycles (Figure S7b). This is the same rate as used in Figure 2 for extended cycling. Interestingly, as opposed to when *d*LTS is cycled over the full 3 to 1 V range, the 2 to 1 V range exhibits drastically more capacity fade. This could be because the 2 to 1 V range includes some diffusive reaction with lithium and therefore, loses some lithium per cycle.

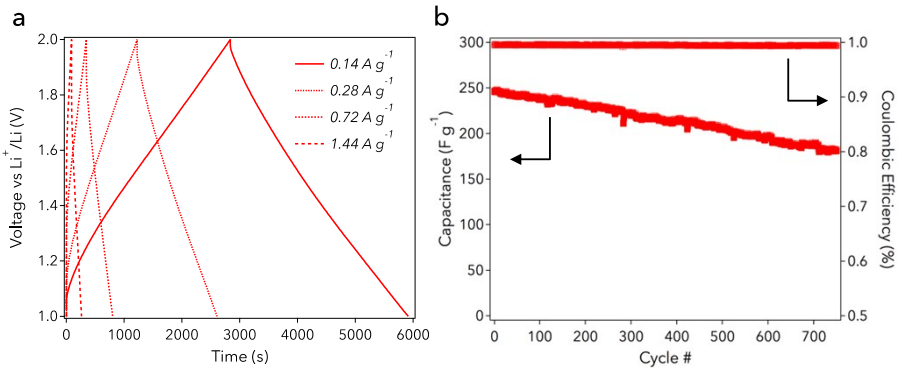


**Figure S7.** a) Voltage vs time for *d*LTS at increasing rates up to 20C. b) Extended cycling at 2C in the 2 to 1 V region. While the current is slightly greater for extended cycling than Figure 3, there is a much larger capacity fade when only using the lower region. This could indicate there is a symbiotic relationship when cycling over the full 3 to 1 voltage range. Perhaps overlap in the diffusive and capacitve regions could be the cause of the greater fade.

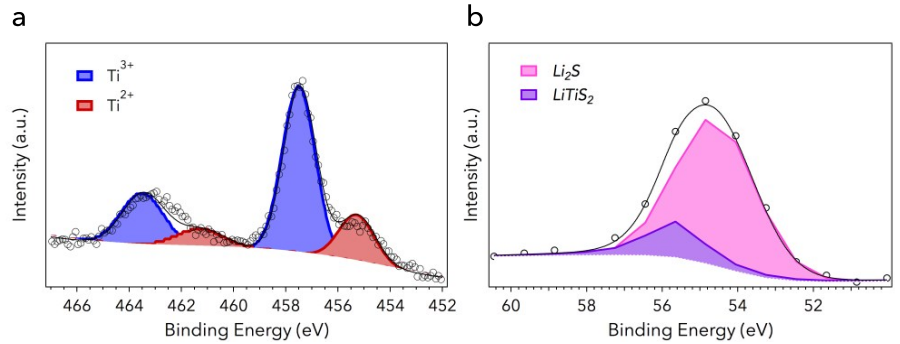


**Figure S8.** Ex-situ XPS spectra at 1 V in *d*LTS for, a) Ti, b) Li. The Ti results clearly indicate a $Ti^{2+}$ state forming in an octahedrally coordinated environment. Li develops an ionic interactions with S.

Theoretically, $TiS_2$ has a specific capacity of 240 mAh $g^{-1}$; calculations for this value assume one mole of lithium per S-Ti-S unit. However, this scenario is only correct if it is assumed the domain size is infinite. Since lithium can only sit in between the $TiS_2$ slabs, once the domain size of the material is significantly reduced, the total number of slabs will become important for calculating a theoretical intercalation capacity. For instance, if the domain size only contains two $TiS_2$ slabs, one mole of intercalated lithium results in a theoretical intercalation capacity of 112 mAh $g^{-1}$. **Figure S9a** displays theoretical calculations for

decreasing domain size of $TiS_2$. Only one the grain size is less than approximately 12 nm or 20 S-Ti-S slabs, does the intercalation capacity significantly differ from the overall capacity. As it is assumed that additional capacity is derived from using surface sulfur coordination at the outer most S-Ti-S slabs in *d*LTS, theoretical calculations have also been included for this amount defined as a "capacitive" contribution. It is clear in Figure S9a that this capacitive contribution only becomes significant at extremely small domain sizes such as the domains identified in Figure 1. The total capacity derived can deviate from traditional studies of $LiTiS_2$ and explain the significant increases developed in Figure 2 and 3.

Figure S9b is the deep discharge characteristics of increasing nano domains of $LiTiS_2$. Beginning with *b*TS, $TiS_2$ is ball-milled with $Li_3N$ for increasing amounts of time – 2, 5, 10, and 20 hours. 2 and 20 already correspond to *n*LTS and *d*LTS, respectively. However, intermediates are developed that have smaller domain sizes than *n*LTS but begin to disorder similar to *d*LTS. All samples are lithiated to 0.01 V at a rate of C/20. Voltage profiles and associated dQ/dV are displayed in Figure S9. First analyzing *b*TS, the discharge characteristics match closely with literature.[8] This is important to note that the same transformation can occur in solid-state as in liquid. The upper region from 2.4 to 1.8 V can uptake a full mole of lithium to form $LiTiS_2$. Then at 0.5 V, the reaction following equation 2 proceeds until another mole of lithium is taken to make the singular phase of $Li_2TiS_2$. The important difference in solid-state is the lack of SEI formation at 0.9 V noted in literature. Finally, the full conversion to $Ti^0$ and $Li_2S$ takes place as in equation 3. It appears the full conversion does not take place as only 3.5 moles of lithium are consumed which is most likely due to the large starting crystallite size of *b*TS. When forming a more nano domain as in *n*LTS (LTS-2h), the upper intercalation region shortens as the unit cell can no longer be counted as infinite (see Figure S9a). Therefore, the theoretical capacity

diminishes. *n*LTS still displays the overintercalated version of $Li_2TiS_2$ in which lithium shifts from octahedral to tetrahedral sites in the van der Waals gap. The final conversion is not as present in *n*LTS which could be blurred by the nano domain size. The trends in LTS-5 to LTS-20 are quite noticeable and provide profound insight into the mechanism of pseudocapacitance. From LTS-5 to LTS-20, the upper intercalation capacity decreases related to a decrease in crystallite size. The amount of pseudocapacitance increases with increasing disorder (lower slope from 2 to 1 V), this is also obvious with higher dQ/dV values. From LTS-5 to LTS-20, the amount of overintercalated plateau shortens until it almost disappears with LTS-20. If surface redox proceeds as the primary pseudocapacitance mechanism, the total overintercalated phase will diminish as lithium will be preferentially stored on the surface of the slab at higher voltages. As there doesn't appear to be any formation of $Li_2TiS_2$ in LTS-20, most likely the domain size is near 5 slabs thick which matches HR-TEM data in Figure 1. Finally, the conversion process still proceeds in LTS-5 through LTS-20. Interestingly, all samples are almost able to fully react with 4 moles of lithium. This is an important concept as developing *d*LTS does not change the final discharge products are ability to store necessarily more lithium. It simply changes the reaction pathway of where lithium preferentially sits over the course of the reaction coordinate. The pseudocapacitive surface redox of S-Ti-S slab becomes more favorable than overintercalation to $Li_2TiS_2$.

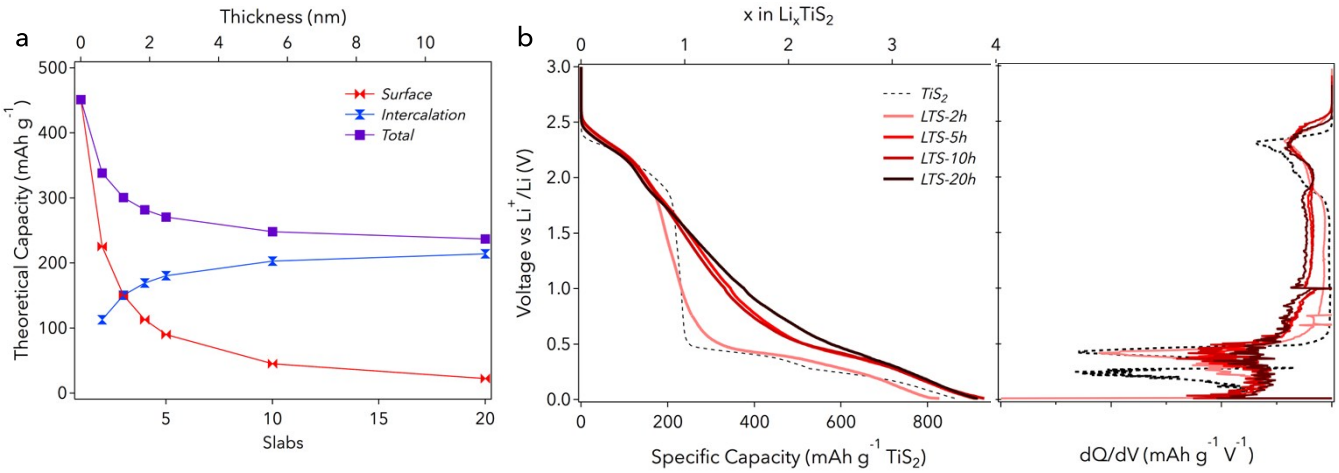


**Figure S9.** a) Calculated specific capacities for extremely small grain sizes in $LiTiS_2$. Diffusive capacities are related to the intercalation of Li into the van der Waals gap. Capacitive contribution is related to coordination on the outer most S-Ti-S slabs. As domain size decreases, more Li can coordinate to the surface states rather than in between the layers. The total capacity using both forms increases the theoretical past the traditional limit of 240 mAh g−1. b) Discharge of $TiS_2$ ball-milled with $Li_3N$ for 0, 2, 5, 10, and 20 hours at a rate of C/20 to 0.01 V following an initial charge of 3 V. Associated dQ/dV is matched to define the reaction plateaus. Whereas *b*TS follows the three reactions in Equations 1 to 3, with increasing milling time (smaller domain size) larger capacitance is derived in lieu of Equation 2 when Ti is reduced to the 2+ state.

If indeed the pseudocapacitance mechanism is surface redox, more surface area would promote more capacity in the lower voltage region. **Figure S10a** displays a cycle at 0.21 mA $cm^{-2}$ for mass loading from 0.75 mg $cm^{-2}$ to 15 mg $cm^{-2}$. Clearly with increasing mass loading, the intercalation region shortens and the pseudocapacitive region elongates. This is an interesting effect so that the same amount of lithium is roughly stored at the 1 V cutoff. This supports the theory of surface redox. This also confirms that the pseudocapacitance is not occurring at the electrode/electrolyte interface as the surface area of contact remains constant but scaling occurs in the z direction and the same overall capacity is achieved.

When working the sulfide family of glass electrolytes, there is always the possibility of electrolyte activation to provide additional capacity.[9] Therefore it is important to check to make sure that the observed pseudocapacitance effect is not influenced by the choice of electrolyte selection. Therefore, the electrolyte composition used for the separator was varied from

77.5$Li_2S$-22.5$Li_2S$ to 60$Li_2S$-40$P_2S_5$ and *d*LTS was discharge (Figure S10b). With decreasing amounts of $Li_2S$ conductivity decreases significantly, which accounts for the increasing ohmic overpotential. However, activation is believed to only take place when the $Li_2S$ content exceeds 75 molar as this supersaturates the glass past the final $Li_3PS_4$ structural unit. In all three cases, pseudocapacitance exists suggesting a product of *d*LTS and not the solid electrolyte.

To further this understanding of possible electrolyte activation, solid electrolyte was used as a separator [2D Interface] (typical construction for all cells in this study) or mixed into the cathode itself with $TiS_2$ [3D Interface]. The cell was then initially charged to observe the capacity derived (Figure S10c). Only activation of the electrolyte occurs in the 3D interface. Since $TiS_2$ contains no lithium, all delithation must occur in the $Li_2S$ in the solid electrolyte. Therefore, we can conclude that electrolyte activation plays no role in all the CVs or cycling occurring in this study.

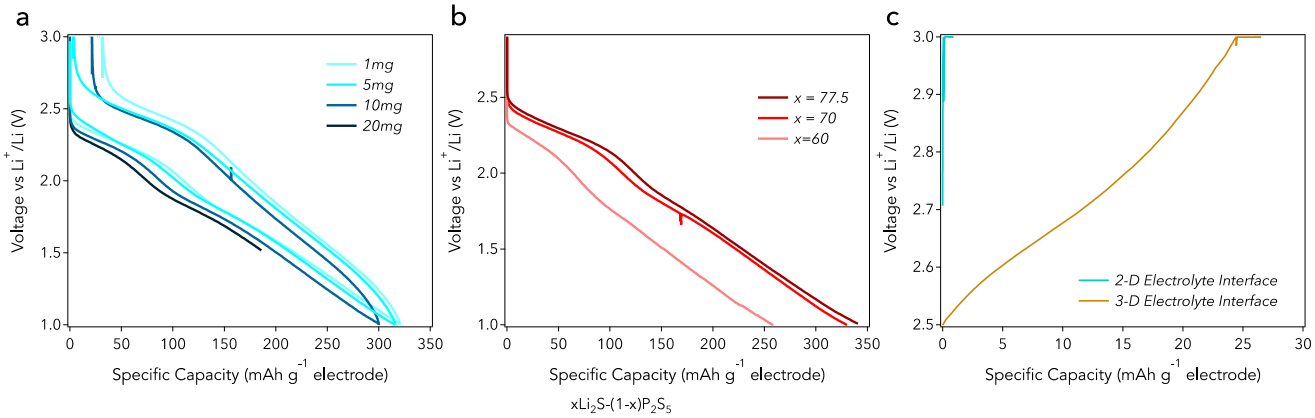


**Figure S10.** a) Increasing thickness of *d*LTS discharged at a rate of 0.21 mA $cm^{-2}$. b) Discharge of *d*LTS on a variety of sulfide solid electrolyte glasses. c) Initial charge of $TiS_2$ mounted or mixed with sulfide solid electrolyte.

**Figure S11** demonstrates the ability of the use of *d*LTS, specifically in the solid-state construction, be "recycled." Figure S11a demonstrates long-term cycling at 1C. Compared to C/2 in Figure 2, *d*LTS degrades at this increased rate. Figure S11b demonstrates the voltage profile

evolution during the first 350 cycles at 1C. The pseudocapacitive region is lost so that only the intercalation portion is providing capacity. This is a different degradation mechanism than *n*LTS in Figure 2. In that case, capacity never became stable and there was in increase in ohmic overpotential. In Figure S11b, there is no ohmic overpotential but simply a loss of pseudocapacitance. Once the system is slowed down to a rate of C/10 and additional pressure is applied, the system recovers full capacity before the degradation. The system is then run for another 200 cycles at 1C before being slowed down to C/10 again to recover capacity. Figure S11c shows the voltage profiles at initial C/10, the first and second recovery. The first and second recovery contain a shorter pseudocapacive region but a lengthening of the intercalation portion. This could indicate there is structural changes in *d*LTS over cycling. The idea of capacity recovery cannot be applied to a liquid cell as SEIs typically form which prevent the reformation of the original structure. However, since an SEI does not form on *d*LTS and the pressure can be finely tuned, the system can be used multiple times in the solid-state.

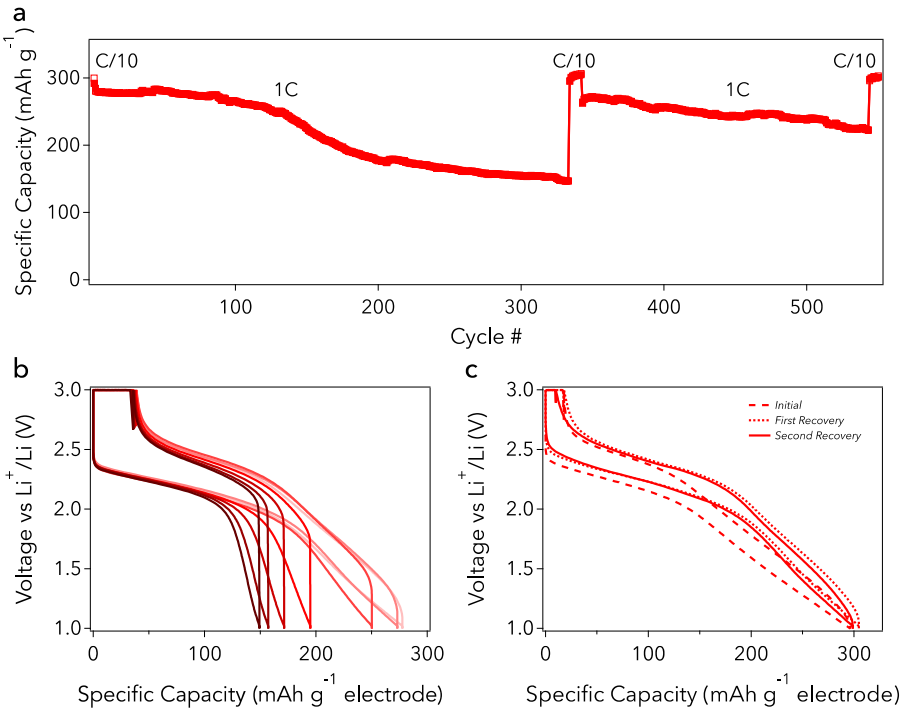

**Figure S11**. a) Cycling of *d*LTS at a 1C rate. The system is slowed down to C/10 and applied additional pressure for 10 cycles. Rate is the increased again to 1C. A second recovery is performed at C/10. b) Voltage profile evolution during the initial capacity degradation at 1C. c) Voltage profiles at C/10 of initial, first recover, and second recovery.

There is curiosity to use *d*LTS at thicker electrodes. Typically, thick electrode cycling is tough to achieve in the solid-state at higher rates due to lack of guaranteed diffusion pathways. **Figure S12** displays cycling of *d*LTS at a 7.5 mg $cm^{-2}$ mass loading (~ 25 μm) and a rate of C/5. The system achieves a stable capacity at 250 mAh $g^{-1}$ which is less than when half the mass loading is used but is still greater than theoretical so the pseudocapacitive effect is preserved for extended cycling at higher mass loadings.

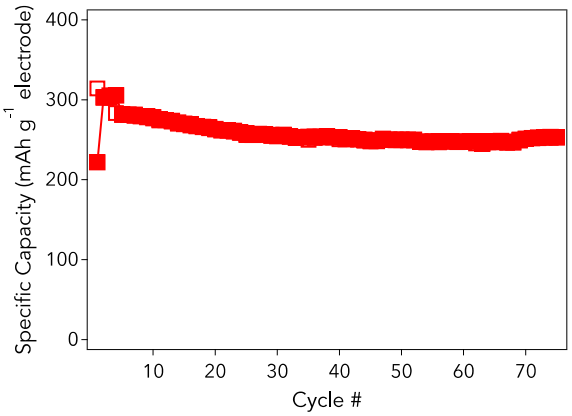


**Figure S12.** Cycling of a 7.5 mg $cm^{-2}$ electrode of *d*LTS at a rate of C/5.

**Supplemental References**


[1] W. Weppner, R. A. Huggins, *J. Electrochem. Soc.* **1977**, 124, 1569.

[2] C. J. Wen, B. A. Boukamp, R. A. Huggins, W. Weppner, *J. Electrochem. Soc.* **1979**, 126, 2258.

[3] A. Van der Ven, J. Bhattacharya, A. A. Belak, *Accounts Chem. Res.* **2013**, 46, 1216; A. Van der Ven, G. Ceder, *J. Power Sources* **2001**, 97-8, 529; A. J. Vaccaro, T. Palanisamy, R. L. Kerr, J. T. Maloy, *Solid State Ion.* **1981**, 2, 337.

[4] S. B. Son, J. E. Trevey, H. Roh, S. H. Kim, K. B. Kim, J. S. Cho, J. T. Moon, C. M. DeLuca, K. K. Maute, M. L. Dunn, H. N. Han, K. H. Oh, S. H. Lee, *Adv. Energy Mater.* **2011**, 1, 1199.

[5] A. J. Bard, L. R. Faulkner, J. Leddy, C. G. Zoski, Electrochemical methods: fundamentals and applications, volume 2. Wiley New York **1980**.

[6] G. A. Muller, J. B. Cook, H.-S. Kim, S. H. Tolbert, B. Dunn, *Nano Lett.* **2015**, 15, 1911.

[7] B. E. Conway, Electrochemical supercapacitors: scientific fundamentals and technological applications. Springer Science & Business Media, **2013**.

[8] D. W. Murphy, J. N. Carides, *J. Electrochem. Soc.* **1979**, 126, 349

[9] T. A. Yersak, C. Stoldt, S. H. Lee, *J. Electrochem. Soc.* **2013**, 160, A1009.